Particle Sorting In a Mini Step-Split-Flow Thin Channel: Influence of Hydrodynamic Shear on Transversal Migration

ARTICLE *in* ANALYTICAL CHEMISTRY · AUGUST 2008

Impact Factor: 5.64 · DOI: 10.1021/ac702579g · Source: PubMed

4 AUTHORS:

N. Callens
European Space Agency
52 PUBLICATIONS **415** CITATIONS
SEE PROFILE

Mauricio Hoyos
École Supérieure de Physique et de Chimie…
57 PUBLICATIONS **511** CITATIONS
SEE PROFILE

Pascal Kurowski
MINES ParisTech
52 PUBLICATIONS **471** CITATIONS
SEE PROFILE

Carlo saverio Iorio
Université Libre de Bruxelles
36 PUBLICATIONS **460** CITATIONS
SEE PROFILE

Anal. Chem. **2008,** *80,* 4866–4875

Particle Sorting In a Mini Step-Split-Flow Thin Channel: Influence of Hydrodynamic Shear on Transversal Migration

Natacha Callens,*,†,‡ Mauricio Hoyos,† Pascal Kurowski,† and Carlo S. Iorio‡

Laboratoire de Physique et Mécanique des Milieux Hétérogènes, PMMH UMR 7636 CNRS, Ecole Supérieure de Physique et de Chimie Industrielles, ESPCI, 10 Rue Vauquelin, 75231 Paris Cedex 05, France, and Microgravity Research Center, Service de Chimie-Physique EP, Université Libre de Bruxelles, 50 Avenue F. D. Roosevelt, B-1050 Brussels, Belgium

A mini splitterless-split-flow thin fractionation (SPLITT) device has been developed to achieve fast separations of micrometer-sized species. In this device, inlet and outlet steps have replaced the splitters, which are common to conventional SPLITT channels. By elimination of the splitters, it becomes straightforward to reduce channel dimensions while maintaining the classic method of fabrication. Reduced dimension channels allow high axial velocity at relatively low flow rate. These high axial velocities generate an enhancement of inertial lift forces and hydrodynamic shear-induced diffusion. Experiments carried out with particulate and biological species in a mini step-SPLITT channel demonstrate that these hydrodynamic effects yield highly enriched fractions of smaller species from binary mixtures.

The preparative technique of split-flow thin fractionation (SPLITT) and the analytical technique of field-flow fractionation (FFF),[1] belong to the separation family of methods which use ribbonlike channels through which separands are axially transported by a laminar flow and transversally driven by an external field force.[2,3] SPLITT fractionation is a fast and easy way to achieve preparative or semipreparative sorting without using filters or dialysis membranes.

In a departure from conventional SPLITT conceived for high throughput, channels of reduced size (mini SPLITT) yield high velocities at relatively low flow rates, generating enrichment through hydrodynamic effects, such as inertial lift forces and shear-induced diffusion, as demonstrated in this paper.

In SPLITT devices, separation is due to a differential migration velocity across the channel thickness, which depends on the interaction between the species and the external field force. Two

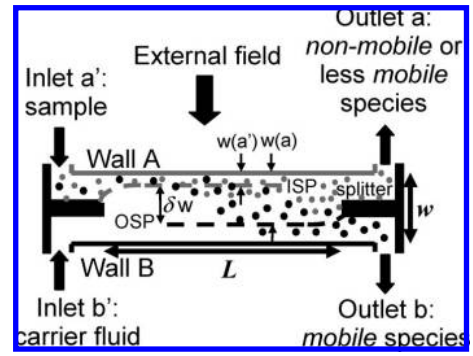

Figure 1. Schematic side view of a SPLITT channel (not to scale).

conventional SPLITT channel geometries currently exist: parallel-plate[4,5] and annular.[6] A side view of the parallel-plate SPLITT channel is shown in Figure 1. By convention, the sample suspension is input at inlet a′ adjacent to wall A, and the carrier fluid (consisting of an inert liquid) is input at inlet b′ adjacent to wall B. Both inlets are separated by an inlet flow splitter that smoothly merges the two incoming substreams. Likewise, an outlet flow splitter divides the flow into two thin fluid lamina for final binary separation at the outlets a and b. In conventional SPLITT devices, the flow splitters occupy about one-third of the channel thickness w, one-fifth of the channel length L (Please note that in Figure 1 the ratio of w to L is greatly exaggerated for illustration.), and the entire channel width B (the dimension perpendicular to the plane of Figure 1). The inlet and outlet splitting planes, named ISP and OSP, are virtual fluid boundaries where, respectively, both inlet substreams merge and both outlet substreams are separated. These planes lie at a distance $w(a')$ and $w(a)$ from wall A. The equation relating flow rates to the ISP position is given by[7]

$$\frac{Q(a')}{Q} = 3\left(\frac{w(a')}{w}\right)^2 - 2\left(\frac{w(a')}{w}\right)^3 \qquad (1)$$

* Corresponding author. Phone: +32 2 650 2982. Fax: +32 2 650 3126. E-mail: natacha.callens@ulb.ac.be.

† Ecole Supérieure de Physique et de Chimie Industrielles.

‡ Université Libre de Bruxelles.

(1) Martin, M.; Williams, P. S. *Theoretical Advancement in Chromatography and Related Separation Techniques*; Dondi, F., Guiochon, G., Eds.; Kluwer Academic Publishers: Dordrecht, The Netherlands, 1992; Vol. 51, pp 3–580.

(2) Giddings, J. C. *Sep. Sci. Technol.* **1985**, *20*, 749–768.

(3) Giddings, J. C. *Science* **1993**, *260*, 1456–1465.

(4) Jiang, Y.; Kummerow, A.; Hansen, M. *J. Microcolumn Sep.* **1997**, *9*, 261–273.

(5) Contado, C.; Blo, G.; Conato, C.; Dondi, F.; Beckett, R. *J. Environ. Monit.* **2003**, *5*, 845–851.

(6) Zborowski, M.; Williams, P. S.; Sun, L.; Moore, L. R.; Chalmers, J. J. *J. Liq. Chromatogr. Relat. Technol.* **1997**, *20* (16–17), 2887–2905.

(7) Springston, S. R.; Myers, M.; Giddings, J. C. *Anal. Chem.* **1987**, *59*, 344–350.

10.1021/ac702579g CCC: $40.75
Published on Web 05/31/2008

with the total flow rate Q,

$$Q = Q(a') + Q(b') = Q(a) + Q(b) \quad (2)$$

where $Q(a')$, $Q(b')$, $Q(a)$ and $Q(b)$ are the flow rate components at their respective inlets and outlets. The OSP position is obtained by replacing $w(a')$ and $Q(a')$ with $w(a)$ and $Q(a)$ in eq 1. The distance between the two virtual planes, $\delta w = w(a) - w(a')$, is called the transport lamina thickness. With ideal geometry and flow, the positions of the ISP and OSP are unaffected by the dimensions and position of the physical splitters and depend only on the flow rate ratios. In the channel between the splitters, the velocity profile $v(x/w)$ across the channel thickness is described by a plane Poiseuille flow for small Reynolds number

$$v\left(\frac{x}{w}\right) = 6\langle v\rangle\frac{x}{w}\left(1 - \frac{x}{w}\right) = 4v_{max}\frac{x}{w}\left(1 - \frac{x}{w}\right) \quad (3)$$

where x is the distance from the channel wall, v_{max} is the maximum fluid velocity found at the channel midpoint and $\langle v\rangle$ is the mean fluid velocity given by

$$\langle v\rangle = \frac{Q}{Bw} \quad (4)$$

Equations 1 and 3 are strictly true for infinite parallel plates and approximately true for typical SPLITT channels where $B \gg w$. It is possible to perform a continuous binary separation as mobile species (large dark particles in Figure 1) are driven by the field force across the transport lamina toward outlet b, while nonmobile or less mobile species (small gray particles in Figure 1) are driven a distance too short to reach the OSP and thus exit at outlet a.

As depicted in Figure 2, parallel-plate SPLITT channels superimpose a stainless steel sheet between two thin Mylar or polyimide sheets. All three sheets have a central rectangular cutout, but the cutout is shorter along the length for the stainless steel sheet. The resulting overhangs give rise to the two flow splitters. These sheets are sandwiched between two glass plates, which form the channel walls. Commercial channels[8] are usually 20 cm long, 4 cm wide, and 0.0380 cm thick. They have a volume of approximately 3 mL, and separation occurs in a few minutes.

The extension of the SPLITT technique to multiseparation and microfluidics becomes challenging if more than two outlets and reduced channel dimensions are needed. In fact, the finite size of the splitters is one of the major difficulties for reducing channel thickness. The other concerns the splitter rigidity. Splitters are easily bent by the pressure difference between adjacent inlet and outlet substreams, and the consequent shape distortion modifies the actual ISP and OSP positions leading to three-dimensional flow nonidealities. Recent studies on annular SPLITT channels[9,10] showed that in the absence of an applied transverse field force, splitter deformations may generate a significant cross stream migration of particles. In order to prevent splitter bending, parallel-plate channels are usually provided with thin Mylar strips between

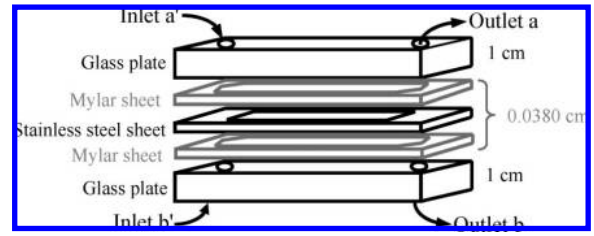

Figure 2. Parallel-plate SPLITT channel fabrication: details of the channel components. The length L is usually 20 cm and the width B 4 cm.

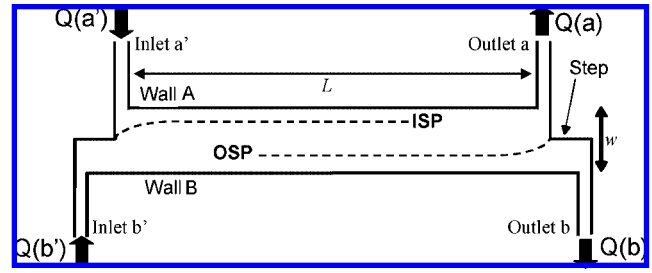

Figure 3. Schematic side view of a step-SPLITT channel (not to scale).

splitters and walls,[8] nevertheless some deformations may remain. Since splitters typically occupy one-third of the channel thickness, there will be an abrupt decrease or increase in mean flow velocity at the open channel entrance or exit, respectively. This gives rise to flow perturbations near the splitter tips. Therefore, if the channel thickness was reduced by decreasing the thicknesses of all three sheets, the system would become more sensitive to splitter deformation. Decreasing the Mylar sheet thickness, while maintaining the splitter thickness to mitigate the problem of splitter deformation, has the confounding result of increasing instabilities due to sudden axial velocity change. While the transport lamina thickness in current environmental applications[9–11] occupies more than one-third of the channel thickness, thereby veiling instabilities due to splitters and their imperfections, thin transport lamina required in biomedical applications such stem cell fractionation[12] makes the system much more sensitive to splitter-induced instabilities.

For all these reasons, it is undoubtedly necessary to remove the splitters to implement a mini SPLITT channel based on the classic method of fabrication. In this experimental work, we used a parallel-plate SPLITT channel, fabricated in-house, of reduced dimensions compared to conventional devices, where splitters are eliminated and replaced by inlet and outlet steps, as shown schematically in Figure 3. This mini splitterless-SPLITT channel, proposed for the first time as a step-SPLITT fractionation device,[13] is composed of two inlets and two outlets and was conceived for conventional SPLITT applications. The steps are formed by two stacked Mylar sheets with different-length cutouts as depicted in Figure 4. As no intermediate stainless steel sheet is required, this architecture allows thinner channels, limited only by the thickness of the Mylar sheets. The height of the step is fixed by the top

(8) POSTNOVA Analytics, Salt Lake City, UT.
(9) Moon, M. H.; Kang, D.; Woon Lee, D.; Chang, Y. *Anal. Chem.* **2001**, *73*, 693–697.
(10) Dondi, F.; Contado, C.; Blo, G.; Garçia-Martin, S. *Chromatographia* **1998**, *48*, 643–654.
(11) Lead, J. R.; De Momi, A.; Goula, G.; Baker, A. *Anal. Chem.* **2005**, *78*, 3609–3615.
(12) Hoyos, M.; McCloskey, K.; Moore, L. R.; Nakamura, M.; Bowell, B. J.; Chalmers, J. J.; Zborowski, M. *Sep. Sci. Technol.* **2002**, *37* (4), 745–767.
(13) Callens, N.; Hoyos, M.; Kurowski, P.; Dubois, F. *11th Symposium on Field-Flow Fractionation*, Cleveland, OH, October 7–10, 2003.

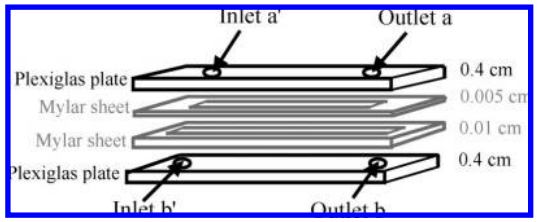

Figure 4. Step-SPLITT channel fabrication: details of the channel components. The length L is usually about 5 cm and the width B about 0.2 cm.

Mylar sheet thickness. As the Plexiglass plates support the steps, problems of splitter bending or misalignment are prevented. The drawbacks of splitter imperfections, including a contribution to nonspecific crossover[14,15] and thus to the loss of separation resolution, are thereby eliminated. These new SPLITT channels are usually about 5 cm long, 0.2 cm wide, and between 0.0100 and 0.0250 cm thick. They can be arranged horizontally or vertically and used in different ways: the sample can be injected from the bottom or from the top, before or after the step, depending on the application. Besides the prototype reported here, only a miniaturized electrical-SPLITT channel without splitters and based on the original Step-SPLITT geometry,[13] has been built but with rather elaborate microfabrication techniques.[16]

The main objective of this work is to take advantage of the enhancement of hydrodynamic effects due to the reduction of the channel volume. Our aim is to study the role played by those effects on the transport process in mini step-SPLITT channels and the possibility of generating separations without any external field. Regarding applications, the mini step-SPLITT channel could be useful for performing separations intermediate in volume between analytical- and preparative-scale. Since the geometry plays a significant role in the fluid dynamics of the system, the next section describes its impact on fluid modeling.

COMPUTER SIMULATIONS

Numerical simulations were performed in order to compare the flow motions in the classical SPLITT configuration with splitters with the new configuration with steps. The two channel architectures were designed and meshed with Gambit software (Fluent Inc., New Hampshire). Simulations were then performed on the 2D geometries using Fluent 6.2.22 (Fluent Inc., New Hampshire), which is a commercial CFD package. The geometries assumed for the simulations were two minichannels of $L = 5.8$ cm, $B = 0.2$ cm, and $w = 0.0325$ cm for the conventional SPLITT and $w = 0.0200$ cm for the step-SPLITT channels, respectively. The thickness difference of 0.0125 cm is due to the existence of a splitter in the former geometry. Note that the conventional SPLITT dimensions have been reduced to obtain a more reliable comparison of the flow behavior in the two geometries. The step thickness is equal to 0.01 cm, which represents half of the channel thickness. Splitter and step lengths were set at 0.5 cm, and their widths correspond to the channel widths. In the step-SPLITT channel inlet a′ and outlet a are situated at the same side of the steps. The numerical meshes have been optimized considering the necessity to recover a fully developed velocity profile in the mini channels. The number of points used is 158 400 for the conventional SPLITT and 150 784 for the step-SPLITT, allowing for having at the same time, mesh cells of different length according to the importance of their positions and an average thickness of ~6 μm. Moreover, some test cases have been performed to evaluate the quality of the mesh. The set of equations solved numerically is

$$\vec{\nabla} \cdot \vec{v} = 0 \tag{5}$$

$$\rho \frac{\partial \vec{v}}{\partial t} + \rho\left(\vec{v} \cdot \vec{\nabla}\right)\vec{v} = \eta \Delta \vec{v} - \vec{\nabla} p + \rho \vec{g} \tag{6}$$

where ρ is the fluid density, η is the dynamic viscosity, p is the pressure, and g is the gravitational acceleration. The boundary conditions prescribed a constant mass flow at the two inlets of the domains, a fixed flow ratio at the outlets, while the no-slip boundary condition was imposed everywhere along the walls. The two equations express, respectively, the mass conservation of the fluid considered as incompressible and the momentum balance.

Taking into consideration that the establishment time of the Poiseuille profile is of the order of $\rho w^2/\eta = 0.04$ s, much smaller than the characteristic experimental time (~0.5 s), the flow has been considered as stationary. The problem was solved using the steady-state solver, implying that the time derivative is omitted in eq 6. In order to have numerical simulations compatible with the experimental setup, the material was prescribed as having physical properties identical to water, the mass flow rate Q ranged between 1 and 3 mL/min, while $Q(a')/Q$ ranged from 0.1 to 0.4 and $Q(a)/Q$ ranged from 0.1 to 0.9. With these settings, a typical simulation takes between 10 000 and 20 000 iterations.

Results of numerical simulations corresponding to the maximum flow rate and $Q(a')/Q = Q(a)/Q = 0.2$, are shown in Figure 5. The calculated average velocity is 7.7 cm/s in the conventional SPLITT channel and 12.5 cm/s in the step-SPLITT channel, which correspond to a Reynolds number of ~25. The path line distribution in the step-SPLITT channel is similar to the conventional one, there is no recirculation at the step vicinity. The ISP and OSP locations correspond to the theoretical predictions (eq 1). This initial fluidic modeling has demonstrated that the new separator should work exactly in the same way as the conventional SPLITT devices. Nevertheless, it is worth noting that even though the step-SPLITT architecture eliminates splitter misalignments, the nonspecific crossover generated by hydrodynamic effects remains, as discussed below.

PARTICLE TRANSVERSAL MIGRATION THEORY

The most common transversal field force used in SPLITT fractionation is gravitational,[9,10] but a few applications involve also magnetic,[17–19] acoustic,[20] and electric[16] fields. Separation times involved in classical applications span generally from one up to several minutes. In this study, the mini step-SPLITT channel volume is 21 μL, which is about 150 times smaller than that of conventional SPLITT devices, typically of 3 mL volume. With the use of flow rates around 3 mL/min, the residence times of particulate species in a mini step-SPLITT channel are very short

(14) Williams, P. S.; Moore, L. R.; Chalmers, J. J.; Zborowski, M. *Anal. Chem.* **2003**, *75*, 1365–1373.
(15) Williams, P. S.; Decker, K.; Nakamura, M.; Chalmers, J. J.; Moore, L. R.; Zborowski, M. *Anal. Chem.* **2003**, *75*, 6687–6695.
(16) Narayanan, N.; Saldanha, A.; Gale, B. K. *Lab Chip* **2006**, *6*, 105–114.

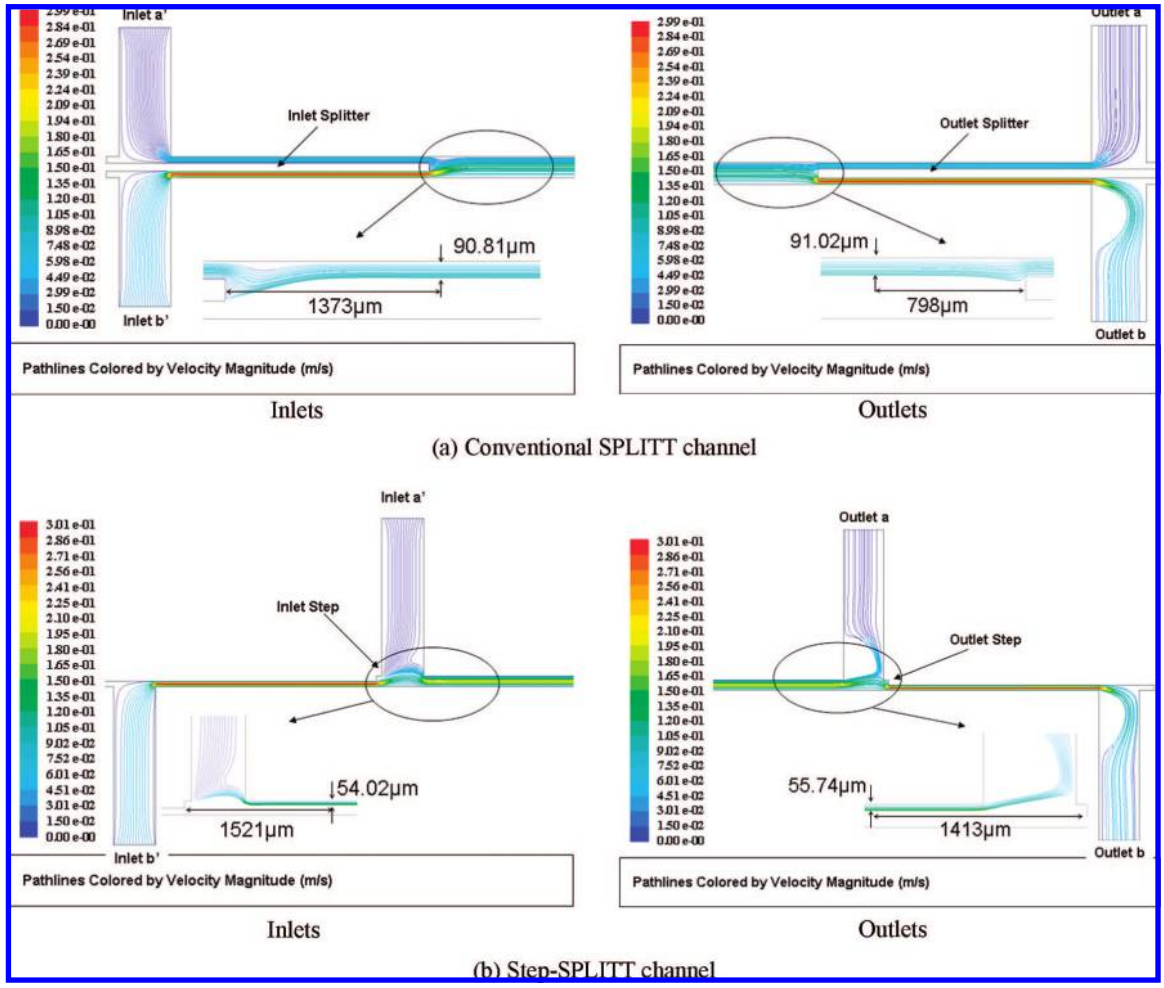

Figure 5. Fluidic modeling results for (a) conventional SPLITT channel and (b) step-SPLITT channel. The path-line distributions are similar. The ISP and OSP have locations corresponding to the theoretical predictions.

(~0.5 s) and the settling distances are of a few particle diameters. The gravitational force is thus not sufficient to be used as a selective force. In contrast, the transversal migration generated by the enhancement of the inertial lift forces and the shear-induced diffusion could be considered as a selective mechanism. Indeed, when the mini step-SPLITT channel is placed vertically and no external transverse field force is acting, these hydrodynamic effects are the only remaining phenomena that can introduce a nonspecific crossover to the sample. In the present paper we focus on this specific situation.

Inertial Lift Forces. It is beyond the scope of this paper to enter into a detailed account of inertial lift forces and their theoretical treatment, but some remarks should be helpful. Inertial lift forces,[21] of a nature different from those of the Magnus forces occurring in inviscid fluids, affect micrometer-sized spherical particles when a hydrodynamic shear flow transports them between parallel bounding walls. They generate a transversal transport which depends on particle radius a, flow velocity v, and a dimensionless distance between the particle and the wall x/w. It is worth noting that so far, a complete theory on inertial lift forces has been developed only for a single particle in linear and quadratic flows.[22,23] A complete model is still lacking because of the complexity in coupling lift forces with other effects, such as shear-induced diffusion, lubrication, etc. In vertical flow, the expression describing these forces states[24,25]

$$F_{\text{lift}} = 6\pi\left(\frac{v_{\max}}{w}\right)^2 a^4 \rho f\left(\frac{x}{w}\right) - \frac{33}{4}\pi U_z v_{\max} a^2 \rho k\left(\frac{x}{w}\right) \qquad (7)$$

where U_z is the particle sedimentation velocity and f and k are polynomial functions:

$$f\left(\frac{x}{w}\right) \approx 19.85\left(0.19 - \frac{x}{w}\right)\left(0.5 - \frac{x}{w}\right)\left(0.81 - \frac{x}{w}\right)$$

$$k\left(\frac{x}{w}\right) \approx \frac{x}{w}\left(0.5 - \frac{x}{w}\right)\left(1 - \frac{x}{w}\right)\left[1 - \frac{5}{2}\frac{x}{w}\left(1 - \frac{x}{w}\right)\right]$$

(17) Bor Fuh, C.; Myers, M. N.; Giddings, J. C. *Anal. Chem.* **1992**, *64*, 3125–3132.
(18) Hoyos, M.; McCloskey, K.; Moore, L. R.; Nakamura, M.; Bowell, B. J.; Chalmers, J. J.; Zborowski, M. *Sep. Sci. Technol.* **2002**, *37* (1), 745–767.
(19) Hoyos, M.; Moore, L. R.; McCloskey, K.; Margel, S.; Zuberi, M.; Chalmers, J. J.; Zborowski, M. *J. Chromatogr., A* **2000**, *903*, 99–116.
(20) Try, N. Ph.D. Thesis, Monash University, Australia, 2003.
(21) Segre, G.; Silberberg, A. *Nature* **1961**, 209–210.
(22) Ho, B. P.; Leal, L. G. *J. Fluid. Mech.* **1974**, *65*, 365–400.
(23) Vasseur, P.; Cox, R. G. *J. Fluid. Mech.* **1976**, *78*, 385–413.
(24) Williams, P. S. *Sep. Sci. Technol.* **1994**, *29* (1), 11–45.
(25) Zhang, J.; Williams, P. S.; Myers, M. N.; Giddings, J. C. *Sep. Sci. Technol.* **1994**, *29*, 2493–2522.

The first term of this expression is independent of gravity, has a maximum value at the wall ($x/w = 0$ and 1), and vanishes at $0.19w$, $0.5w$, and $0.81w$. Theoretical predictions[22–24] and experimental results[25] indicate that, regardless of size and under conditions where no other forces act upon particles, the channel midpoint is unstable, while the two other locations are equally stable equilibrium positions.

The second term of this expression is gravity dependent. When gravity is acting in the flow direction (U_z is positive and the second term is negative in eq 7), this contribution to the inertial lift forces pushes particles toward the channel walls. When gravity is acting opposite to the flow direction (U_z is negative and the second term is positive in eq 7), the lift force pushes particles toward the channel center. To compare the magnitude of these two terms for a typical particle of 10 μm diameter and 2.5 g/cm^3 density, at $x/w = 0.1$ the gravity-dependent term is around 1.8×10^{-8} dynes while the gravity-independent term is about 6.2×10^{-7} dynes. Thus the gravity-dependent inertial lift force is negligible compared to the gravity-independent force.

Inertial lift forces as selective forces for separating particles have been used in FFF[1] and SPLITT fractionation. In FFF, high-resolution analytical size fractionation has been obtained by combining inertial lift and gravity forces. Separation of latex mixtures (from 5 to 20 μm in diameter) was realized in an 80 μm thick and 36 cm long separation channel.[26] In SPLITT fractionation, experiments made with polystyrene latex particles (from 10 to 50 μm in diameter) in channels of short length (2 and 10 cm) show that inertial lift forces allow the separation of particles according to their size.[25] The resolution was found to be smaller than that predicted theoretically. On one hand, this is due to the uncertainties regarding the critical alignment and rigidity of the splitters, and on the other hand, probably because of the high particle size-to-channel thickness ratio (50 μm/330 μm = 0.15), which locally modified the flow profile leading, therefore, to a modification of the inertial lift force.

Shear-Induced Diffusion. In SPLITT fractionation, when injected into the channel, the sample is confined in a zone between the wall and the ISP. In this zone, species undergo a high shear rate. Species traveling at different transversal positions are thus transported at different axial velocities. In these conditions, hydrodynamic and steric particle−particle interactions lead to a modification of the microstructure of the particle cloud, generating transversal displacements of species away from their original streamlines. This is a randomlike phenomenon which leads finally to an effective transversal transport along the channel thickness. This nonspecific crossover is known as the hydrodynamic shear-induced diffusion (HSID).[27–29] This effect has been described and studied mostly for concentrated suspensions,[29] even though measurements verify that it also exists in dilute disperse media.[30] The HSID is characterized by the diffusion coefficient:[28,29]

$$D_h = c\dot{\gamma}a^2 h(\varphi) \tag{8}$$

where c is a constant, $\dot{\gamma}$ is the shear rate, and $h(\varphi)$ is an increasing function of the particle volume fraction φ. As this diffusion coefficient is proportional to the square of the particle radius, it could generate some transverse selectivity.[31,32] Two types of diffusion phenomena are reported in the literature: the self-shear-induced diffusion[28,33] and the concentration gradient shear-induced diffusion.[34] The former is related to the migration of one particle in a sheared homogeneous suspension. This target particle migrates in the shear rate direction because it suffers a series of random hydrodynamic interactions with other particles leading to an effective diffusive-like displacement. Equation 8 quantifies this effect. The second diffusion process appears when concentration gradients are originally present in a shear flow. The diffusion here is a collective effect: particles migrate from high to low concentration zones generating a front of diffusion. This Fick-like diffusion is characterized by a coefficient D_c which can be determined experimentally by measuring the displacement l of the front of diffusion as $(2D_c t)^{0.5}$. In both cases of diffusion, the initiating mechanism is the same: the shear flow. Expressions are available in the literature for Fickian diffusion, and these are by default used to evaluate D_c. The only expression that is commonly used to describe HSID, as such, is given by eq 8.[28,29] Several coefficients have been proposed for this expression, but the function $h(\varphi)$ is not still fully determined. Recent studies suggest that h has a linear dependency in φ in the dilute case. Equation 8 proposed by Acrivos gives in our case, with $c = 0.036$ and $h(\varphi) = \varphi$, a value of D_h around 3×10^{-8} cm^2/s, which would correspond to a diffusion length of a few micrometers. This value is too small to account for the transversal migration observed experimentally. Nevertheless, all literature reports of experiments with monodisperse suspensions give concentration gradient shear-induced diffusion coefficient values 2 orders of magnitude higher than the theoretical prediction for the self-shear-induced diffusion coefficient, without giving detailed explanations.[35–37] In addition, in the case of shear-induced diffusion of bidisperse suspensions, experiments show segregation, suggesting an increasing of the average diffusion effect of at least a factor of 3.[31,32]

By taking into account the current knowledge of the inertial lift forces and the shear-induced diffusion, we might assume that the nonspecific crossover observed in a step-SPLITT channel without an external transversal field force is due to a complex coupling of these hydrodynamic effects. In the next section we present experiments which attempt to demonstrate that this can lead to sample purification.

EXPERIMENTAL SECTION

The mini step-SPLITT channel used in this work was 0.18 cm wide, 6.5 cm long, and 0.0184 cm thick corresponding to a volume of 21 μL. It was assembled by overlaying two Mylar sheets 100

(26) Pazourek, J.; Chmelik, J. *Chromatographia* **1993**, *35* (9−12), 591–596.
(27) Eckstein, E. C.; Bailey, D. G.; Shapiro, A. H. *J. Fluid. Mech.* **1977**, *79*, 191–208.
(28) Leighton, D.; Acrivos, A. *J. Fluid Mech.* **1987**, *181*, 415–439.
(29) Leighton, D.; Acrivos, A. *J. Fluid. Mech.* **1987**, *177*, 109–131.
(30) Zarraga, I. E.; Leighton, D. *Phys. Fluids* **2002**, *14* (7), 2194–2201.
(31) Krishnan, G. P.; Beimfohr, S.; Leighton, D. *J. Fluid Mech.* **1996**, *321*, 371–393.
(32) Krishnan, G. P.; Leighton, D. *Int. J. Multiphase Flow* **1995**, *21* (5), 721–732.
(33) Breedveld, V.; van den Ende, D.; Jongschaap, R.; Mellema, J. *J. Chem. Phys.* **2001**, *114* (13), 5923–5936.
(34) Phillips, R. J.; Armstrong, R. C.; Brown, R. A.; Graham, A. L.; Abbott, J. R. *Phys. Fluids A* **1992**, *4* (1), 30–40.
(35) Lopez, M.; Graham, D. M. *Phys. Fluids* **2007**, *19*, 1–10.
(36) Salhi, D., Ph.D. Thesis, Université Paris VII, France, 2006.
(37) Contado, C.; Hoyos, M. *Chromatographia* **2007**, *65*, 453–462.

and 50 μm thick, sandwiched between two bolted Plexiglas plates. For prevention of leaks, Neoprene glue was used between the plates and the Mylar. Digital holographic microscopy[38,39] shows that the glue increases the channel thickness by 34 μm. The offset between the two inlets and the two outlets was 0.5 cm, and the step thickness was 67 μm. Even though gravitational effects are predicted to be negligible, the channel was mounted vertically with flow in the downward direction in order to prevent transversal sedimentation. Two syringe pumps (KDS 100, KD Scientific Inc., Massachusetts) provided independent substreams at the inlets a′ and b′. The outlet flow *a* was controlled by a withdrawal syringe pump (KDS 120, KD Scientific Inc., Massachusetts), while the outlet flow b was free and its flow rate governed by mass conservation (eq 2). Experiments were carried out at a total flow rate Q ranging from 1 to 4 mL/min which correspond to a mean velocity v between 4.53 and 18.12 cm/s (eq 4). The fractional sample flow rate $Q(a')/Q$ was fixed at 0.1 or 0.2, and $Q(a)/Q$ varied from 0.15 to 0.5. SPLITT systems are generally operated in continuous mode, but for practical purposes, the sample was introduced in pulses via a six-way injection valve (model 7050, Rheodyne LLC, Cotati, CA) fitted with a 40 μL loop which corresponds to about twice the channel volume. Three kinds of mixtures were investigated. Two were composed of binary mixtures of 5 and 8 μm and 5 and 10 μm diameter silica particles (Duke Scientific, Palo Alto, CA) of 2.5 g/cm^3. These mixtures were suspended in double distilled, deionized water to obtain a volume fraction of 0.5%. The last sample was composed of a mixture of *Bacillus subtilis* bacteria (Sigma-Aldrich Co., St. Louis, MO) and *Saccharomyce cerevisiae* yeast (Gist-Brocades, Caserta, Italy) suspended in phosphate buffered saline (PBS) to obtain a volume fraction of 0.5%. The goal was to enrich one collected fraction with one of the two species comprising the injected mixture. The size distribution of injected samples and collected fractions was determined by a Z2 Coulter counter (Beckman-Coulter Inc., California). Also, Coulter counts gave the number of each species injected in the system and retrieved in the two collected fractions. This information permits the calculation of the purity (the relative number of either species in each fraction), the concentration (the number of particles per milliliter), the outlet retrieval fractions, and the losses in the system. Experiments were performed in triplicate, and each collected fraction was counted at least three times.

RESULTS AND DISCUSSION

In conventional SPLITT fractionation, the retrieval fraction of a monodisperse population, for example, F(a) for outlet a, is defined as the ratio of the mass of particles collected at the outlet to the total injected mass.[40] For experiments involving binary mixtures, the two species should be differentiated by determining purities and concentrations. In this study, the collected particle number is not a relevant parameter because a limited number of particles is injected in a short time. In practical situations, the SPLITT channel is used in continuous mode, and the pertinent parameters indicating the performance of the separator are the purity and concentration.

For this reason, the Z2 Coulter counter was used, as previously noted, to calculate the following purities:

$$\begin{cases} P(a,1) = \dfrac{n(a,1)}{n(a,1)+n(a,2)} = 1 - P(a,2) \\ P(a,1) = \dfrac{n(a,1)}{n(a,1)+n(a,2)} = 1 - P(a,2) \end{cases} \quad (9)$$

$P(a,1)$ is the purity of species of type 1 at outlet a, and $n(a,1)$ is the number of species of type 1 at outlet a. The purities of species 2 could be explicitly defined by replacing "1" with "2" in the above equation. For the binary mixtures, species 1 will refer to the smaller particles. In what follows, we always shall indicate purities in percentage.

Experiments have been conducted at different flow rates and at different transport lamina thicknesses. Figures 6, 7, and 10 show horizontal histograms representing, for each outlet flow rate ratio $Q(a)/Q$, purities in outlets a and b (in %). Gray bars correspond to smaller species and white bars to larger ones. In each bar, the species size and concentration, in particles per milliliter, are indicated. Bottom horizontal bars show injected purities. On the bottom of each plot, Q and $Q(a')/Q$ values are given and the experimental conditions are schematized.

Evidence of Particle Size Selectivity. As a general result, the mini step-SPLITT channel appears to generate an enrichment, meaning that $P(a,1) > P_0(a,1)$ where $P_0(a,1)$ is the purity of small species of the injected sample. The injected mixture of 5 and 8 μm silica particles was composed of 50% in number of each species and the experiments were conducted at $Q(a')/Q = 0.2$. The best enrichments were obtained for total flow rates $Q = 2$ and 3 mL/min and for small or negative transport lamina thickness δw (when $Q(a)/Q < Q(a')/Q$). As expected, the enrichment in outlet a of small particles tends to decrease with increasing transport lamina. Figure 6a shows that for $Q = 2$ mL/min and $Q(a)/Q \leq 0.225$, $P(a,1)$ varied from 90 to 98.5%, which means that outlet a contained primarily 5 μm particles. In contrast, $P(b,1)$ varied from 42 to 48% but the error bars of the particle purities in outlet b do not allow us to conclude an enrichment in 8 μm particles. The concentration of 5 μm particles in outlet a are on the order of 10^3 particles/mL, namely, 1 order of magnitude less than in outlet b.

Figure 6b shows that for $Q = 3$ mL/min and $Q(a)/Q \leq 0.225$ the results are similar: in outlet a, a very good enrichment of 5 μm particles is obtained while at outlet b, within the errors bars, no significant enrichment in 8 μm particles is observed. The only difference is that in this experimental case the concentration of 5 μm particles in outlet a is higher, of the same order of magnitude as in outlet b. The results obtained for the mixture of 5 and 10 μm diameter silica particles are plotted in Figure 7. The injected sample was composed of 70% in number of small particles and 30% of large particles. This proportion was fixed in order to keep the relative volume fraction of smaller particles similar to that of the previous mixture of 5 μm and 8 μm (around 20%). In fact, hydrodynamic interactions depend rather on total volume fraction than on particle concentration. The experiments were performed at $Q = 3$ mL/min and $Q(a')/Q = 0.2$. The histogram shows that for a negative transport lamina thickness, an important enrichment in small particles is obtained at outlet a: $P(a,1)$ varied from 90 to

(38) Dubois, F.; Callens, N.; Yourassowski, C.; Hoyos, M.; Kurowski, P.; Monnom, O. *Appl. Opt.* **2006**, *45* (16), 3893–3901.
(39) Callens, N. Ph.D. Thesis, Université Paris VI, France, and Université Libre de Bruxelles, Belgium, 2005.
(40) Williams, P. S.; Levin, S.; Lenczycky, T.; Giddings, J. C. *Ind. Eng. Chem. Res.* **1992**, *31*, 2112–2181.

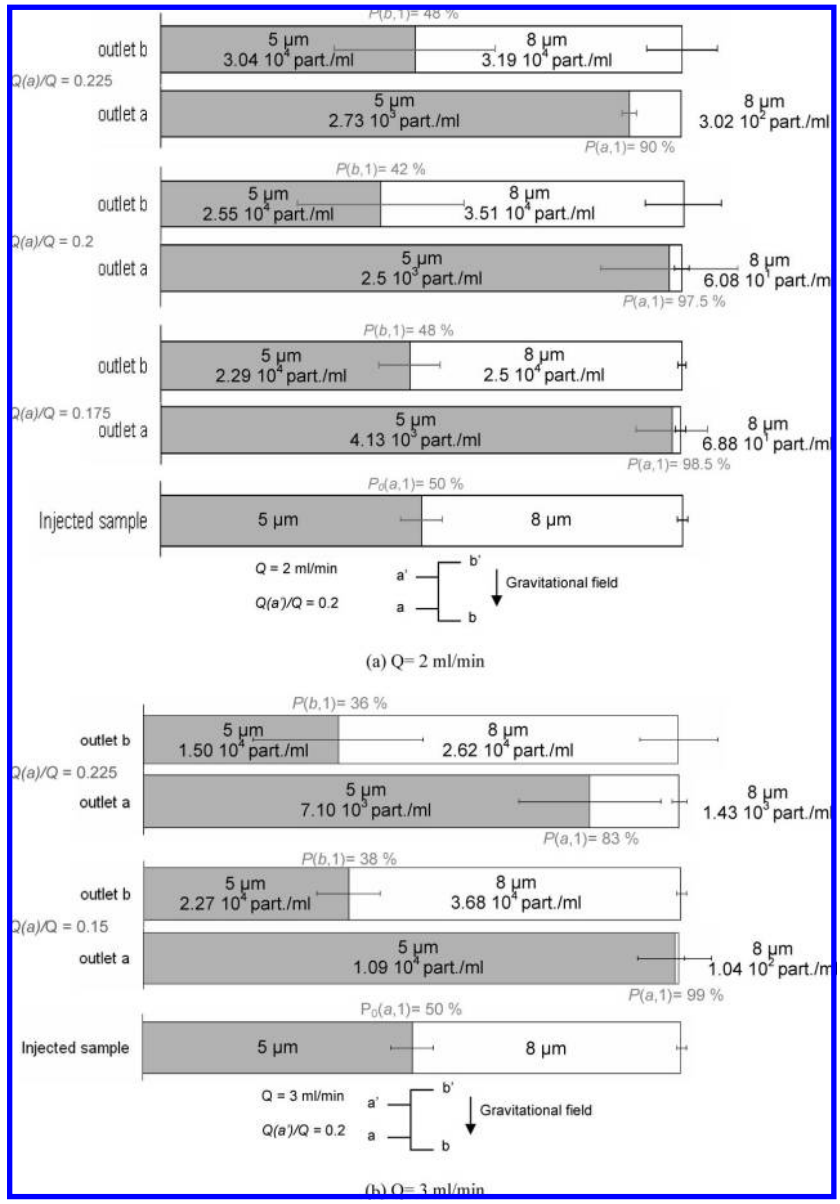

Figure 6. Plot showing the composition of the injected mixture of 5 and 8 μm diameter particles and of the collected fractions at the two outlets in a mini step-SPLITT channel set vertically without an external transversal field force. (a) $Q = 2$ mL/min and (b) 3 mL/min and $Q(a')/Q = 0.2$.

97%, but within the errors bars, no significant enrichment in 10 μm particles is observed at outlet b (P(b,1) varied from 70 to 80%). The concentration of small particles is of the same order of magnitude in both outlets.

On average for the two mixtures, the loss of species was around 60%. It is worth noting that most of the loss occurs in connections, tubing, and dead volumes, with loss in the channel being always less than 5%. We determined those values by short-circuiting the channel and connecting inlets directly to outlets. The aim of these experiments was to demonstrate the possibility of increasing the purity of at least one species by using only hydrodynamic effects. Thus, the recovery, the number of a particular species recovered in an outlet normalized by the number of that species injected, is not calculated. This aspect deserves a particular study in a forthcoming paper dedicated to losses in separation channels.

Our concern in this study was related to selective losses and to try to maintain the relative sample composition during the sorting process. By looking at the total recovery, we realized that the proportions of each species obtained in outlet mixtures were slightly different: the first collected mixture (5 and 8 μm) contained 45% of 8 μm species instead of 50% (in the injected sample), and the second collected mixture (5 and 10 μm) 15% of 10 μm particles instead of 30% (in the injected sample). This selective loss of larger particles is included in the errors bars showed in Figures 6 and 7 and does not significantly affect the purities.

Nature of the Transverse Transport. The fact that without an external transversal field force almost all larger particles elute at outlet b demonstrates that hydrodynamic effects must be considered responsible for the nonspecific crossover. Indeed, results show clearly that larger particles are migrating farther from

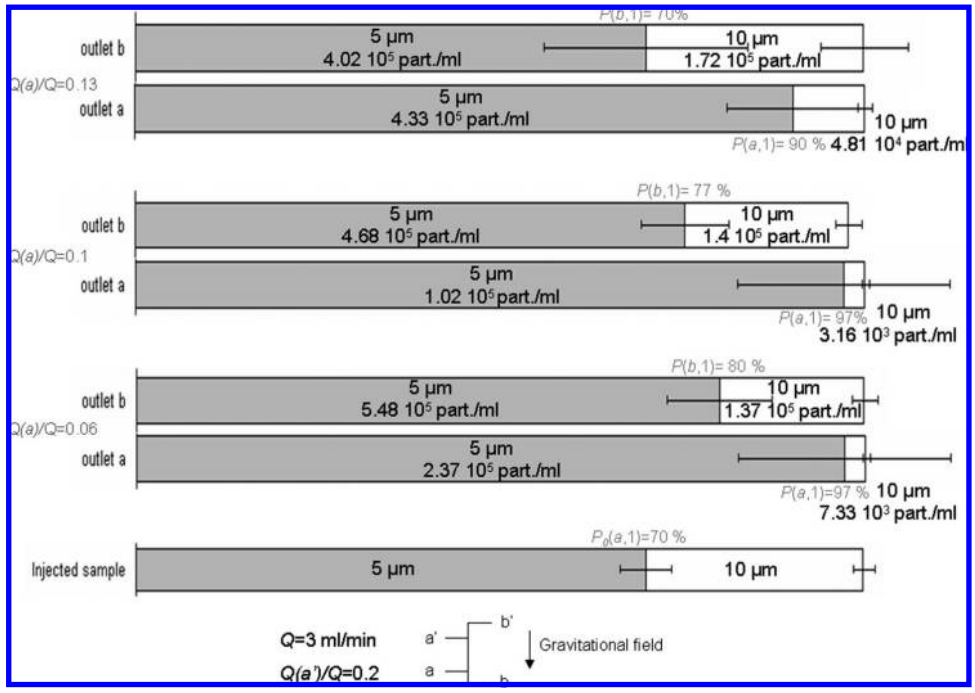

Figure 7. Plot showing the composition of the injected mixture of 5 and 10 μm diameter particles and the collected fractions at the two outlets in a mini step-SPLITT channel, set vertically without an external transversal field force. $Q = 3$ mL/min and $Q(a')/Q = 0.2$.

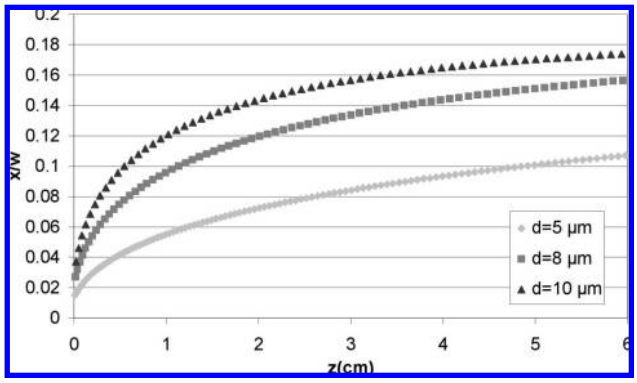

Figure 8. Plot of the trajectories of isolated particles of 5, 8, and 10 μm diameter flowing inside the mini step-SPLITT channel computed by using eqs 3 and 7. Results show clearly that larger particles are migrating farther from the injecting wall, and that inertial lift forces alone should not drive particles beyond $0.2w$.

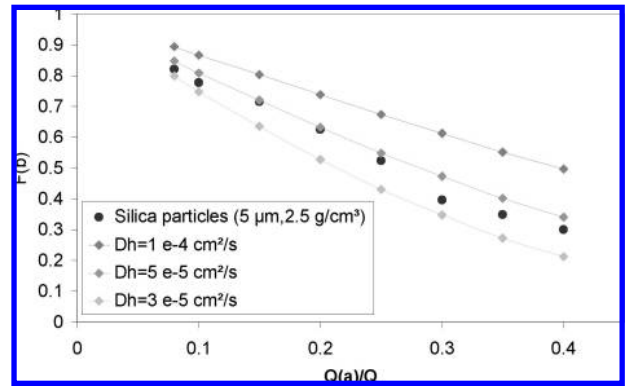

Figure 9. Comparison of theoretical and experimental retrieval fractions F(b) at different flow rate ratio $Q(a)/Q$. Experiments have been realized with 5 μm silica particles at $Q(a')/Q = 0.2$ and $Q = 3$ mL/min in the mini step-SPLITT channel. The theoretical curve has been determined by numerically solving the convection-diffusion equation as a function of the adjustable parameter D_h.

the injecting wall. Nevertheless as previously reported (see theoretical section) inertial lift forces alone should not drive particles beyond $0.2w$, which corresponds approximately to a flow rate ratio of 0.1 (eq 1). Figure 8 shows calculated flow trajectories of isolated particles of 5, 8, and 10 μm diameter flowing inside the mini step-SPLITT channel, computed with the aid of eqs 3 and 7. It is assumed that the particles are initially against the wall at $z = 0$, with the gray plots corresponding to particle centers. We observe that at the exit of the channel, the trajectories do not reach the equilibrium position of $0.2w$. The final position of the 8 and 10 μm particles are close to each other ($0.156w$ and $0.173w$, respectively) and separated by about 9 μm from the final position of the 5 μm particles. This distance is too small to explain, by itself, the segregation observed in Figures 6 and 7.

The possibility of shear-induced diffusion acting concurrently with inertial lift forces has to be considered. To better evaluate the diffusive-like character of the transport process, the experimental and theoretical retrieval fraction F(b) at various flow rate ratios $Q(a)/Q$ have been compared and reported in Figure 9. Experiments have been performed with 5 μm silica particles at $Q(a')/Q = 0.2$ and $Q = 3$ mL/min in the mini step-SPLITT channel. Theoretical curves have been determined by numerically solving the convection-diffusion equation in the stationary regime:

$$\frac{\partial \varphi}{\partial z} = \frac{D}{v(x)} \frac{\partial^2 \varphi}{\partial z^2} \tag{10}$$

We proceed as Williams et al.,[40] which used the Crank−Nicolson finite difference method with the boundary conditions adapted to SPLITT configuration to predict separation of macromolecular

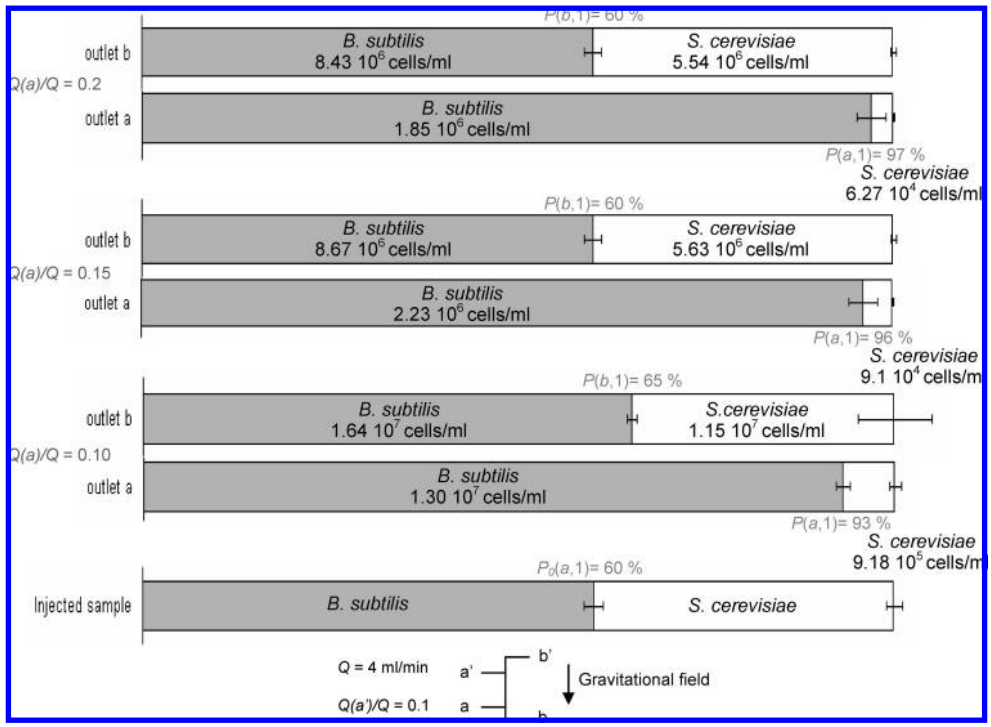

Figure 10. Plot showing the composition of the injected mixture of *B. subtilis* and *S. cerevisiae* and the collected fractions at the two outlets in a mini step-SPLITT channel, set vertically without an external transversal field force. $Q = 4$ mL/min and $Q(a')/Q = 0.1$.

samples as a function of their diffusion coefficients.[40,41] From eq 10, the profile of concentration, mass, or volume fraction, between the wall and the OSP, can be determined. With the use of the appropriate integration boundaries, F(a) and F(b) can be deduced and for a given D_h and they can be plotted as a function of $Q(a)/Q$. Our approach consisted of considering D_h, in this case the hydrodynamic shear-induced diffusion coefficient, as an adjustable parameter. The assumption is that the noncolloidal suspensions have a diffusion-like behavior, enabling them to be treated in the same theoretical structure as macromolecular systems. The shear-induced diffusion of particles and molecular diffusion of macromolecules, operating in SPLITT channel geometry, generates a transversal migration away from the wall resulting in nonspecific crossover. Figure 9 shows a series of theoretical curves F(b) vs $Q(a)/Q$ plotted for different values of D_h. We observe that all experimental values are located between curves corresponding to $D_h = 10^{-5}$ and 5×10^{-5} cm^2/s. This derived D_h value is 3 orders of magnitude larger than the value calculated from eq 8. In the literature, as mentioned before, experimental D_h values[35] are also found to be larger than theoretical prediction by at least of 2 orders of magnitude. However, those experiments were performed at a very low shear rate 2−100 s^{-1} compared to ours performed at greater than 10^3 s^{-1}, which could explain the difference. Moreover, since inertial lift forces were neglected, there will be a slight overestimation of optimal D_h.

We may conclude that experimental results clearly show a shear-induced diffusion behavior, even though the coupling with the inertial lift forces remains unknown.

***Bacillus subtilis* and *Saccharomyces cerevisiae*.** As the mini step-SPLITT channel has been constructed mainly for biological applications, the capability of sorting biological mixture by hydrodynamic effects has been tested in this study. A sample composed of 60% in number of *B. subtilis* and 40% *S. cerevisiae* has been prepared. The idea was to use this synthetic mixture, easy to prepare, to check the ability of the mini step-SPLITT channel to separate cells of distinct diameters. A Coulter counter distribution shows that *B. subtilis* has an equivalent spherical diameter ranging from 1 to 2.5 μm and *S. cerevisiae* from 2.5 to 5.5 μm. The separation results obtained for this biological mixture are reported in Figure 10. As both species are smaller than the silica particles used for the two previous experiments, a larger total flow rate, $Q = 4$ mL/min, was required to induce significant hydrodynamic effects. The experiments were conducted at $Q(a')/Q = 0.1$, and $Q(a)/Q$ varying from 0.1 to 0.2. In each case, $P(a,1) \geq 93\%$, which means that the fractions collected at outlet a contained nearly pure *B. subtilis*. At outlet b, the composition remains similar to the injected sample. The concentrations of *B. subtilis* in outlet a are of the same order as that in outlet b and much higher than for particulate material. It is worth noting that in the biological sample, the loss of species in the system was less than 30% and that the proportions of each species in outlet mixtures remained similar to those of the injected sample. The lower loss compared to particle mixtures is probably due to the weaker electrostatic interaction between the biological species and the tubing.

These results allow concluding that the same hydrodynamic effects operating with particulate species also operate with biological species. Hydrodynamic effects should permit the separation of a mixture of biological species with different hydrodynamic diameter.

CONCLUSIONS

We explored the hydrodynamic effects affecting the transport of micrometer-sized species in a mini SPLITT channel without

(41) Fuh, C. B.; Levin, S.; Giddings, J. C. *Anal. Biochem.* **1993**, *208*, 80–87.

splitters, which were replaced by steps. The mini step-SPLITT geometry permits the scale-down of the separator without abandoning the conventional fabrication method and prevents the problems of splitter bending or misalignment and flow instabilities at the splitter tip, which often plague conventional channels. Reducing the channel dimensions yields high flow velocities and high shear rates at reasonable flow rates, which theoretically should generate an enhancement of inertial lift forces and shear-induced diffusion. From our experimental results, we conclude that lift forces calculated from equations applicable to a single particle are not enough to predict measured segregation but lift forces of interacting particles remain unknown. We have demonstrated, however, that shear-induced diffusion is the main cause of nonspecific crossover in the mini step-SPLITT channel. Experimental results show that high-purity fractions of the smaller species in binary particle and cell mixtures may be obtained by exploiting shear-induced diffusion, even though it is coupled with lift forces. The ideal situation would be to have in outlet a the highest purity and the larger ratio (concentration in outlet a to concentration in outlet b) of one species. The results for the smallest species reported in this paper readily fulfill the first condition, and the second one is found to be close to 1. We do not know any report in the literature of separation in this range of size to compare with. We consider that when operated in continuous mode, the concentration may give a reasonable absolute species number recovery. In addition, the collected fraction in outlet b can be reinjected in order to increase the species recovery.

ACKNOWLEDGMENT

This work was supported by the SSTC/ESA-PRODEX (Services Scientifiques Techniques et Culturels/European Space Agency-Programmes de Développement d'Expériences) Contract 90171, the CNES (Centre National d'Etudes Spatiales), and by the CGRI (Commissariat Général aux Relations Internationales de la Communauté Française de Belgique) Tournesol Program (2005−2006). We thank Michel Martin and Lee Moore for helpful discussions.

Received for review December 20, 2007. Accepted April 14, 2008.

AC702579G